Recent Innovations in Mechatronics (RIiM) Vol 10. (2023) No 1.
DOI: 10.17667/riim.2023.02

Simulation of PMSM Vector Control Using Multisim and LabVIEW

Amro Mohamed Hafez Abdelrazek Khaled
University of Debrecen, Faculty of Engineering,
Department of Mechatronics
amr222@mailbox.unideb.hu

Péter Tamás Szemes
University of Debrecen, Faculty of Engineering,
Department of Mechatronics
szemespeter@eng.unideb.hu

***Abstract*. This paper represents the simulation of field-oriented control of a permanent magnet synchronous motor. Using Clark-Park transform and three PI controllers for controlling speed, direct-axis current, and quadrant axis current. As maximum torque occurs when the rotor field and stator fields are 90 degrees from each other. The goal is to bring the stator field always orthogonal to the rotor field. The simulation is performed using Multisim and LabVIEW software.**

Keywords. PMSM, PI Controller, PWM, Vector control, FOC, Clark-Park transform, ISE, IAE.

I. INTRODUCTION

Similar to brushless DC motors (BLDC), permanent magnet synchronous motors (PMSM) are rotating electrical machines with wound stators and permanent magnet rotors that give sinusoidal flux distribution throughout the air gap. This is the primary distinction between PMSM and BLDC, as the back EMF of the latter has a trapezoidal form.

PMSM can be divided into two categories based on how magnets are attached to the rotor: surface PMSM (SPMSM) and interior PMSM (IPMSM). All magnets are surface mounted in SPMSM, Where in IPMSM, the magnets are placed inside the rotor.

The paper aims to simulate vector control for PMSM using Multisim and LabVIEW. It's organized as follows. The specification of the model which includes the nominal values, primary application, loads, and test conditions is described in section II. Section III describes the system model and description of its components such as the electrical machine, inverter, sensors, and controllers and it includes a description of the performance metrics. Section IV will describe the Experiment and tests performed, steady-state operation, controller tuning, and test conditions. In section V there will be an evaluation of controller tuning and test conditions. Finally, the conclusions are summarized in section VI.

II. SPECIFICATION OF THE MODEL

Nominal Values of the Chosen Motor

The nominal values of the chosen PMSM model, load, and test conditions are described in table I. We've selected Siemens 1FT7136-5AB71 three-phase PMSM. This motor is intended for industrial or commercial plants, it's designed for operation in sheltered areas under normal climatic conditions. It has low torque ripple, and it achieves extremely good dynamic performance and very short cycle times due to its low rotor inertia, the cooling method used is forced ventilation [1].

TABLE I. NOMINAL VALUES OF THE PMSM

Parameter	**Nominal value**		
	Number	***Unit***	***Symbol***
Pole pairs	4	-	p
Stator resistance	0.103	Ω	Rs
Direct-axis Inductance	3.9×10^{-3}	H	L_d
Quadrant-axis inductance	3.9×10^{-3}	H	L_q
Shaft inertia	748×10^{-4}	$Kg.m^2$	J
Rated Current	25	A	I
Rated Speed	1500	rpm	$\dot{\theta}$
Flux linkage	0.4971	Wb	ψ
Inverter Voltage DC	600	V	V_{dc}
PWM frequency	100	kHz	f
Load	91	N.m	T
Power	14.5	kW	P

III. SYSTEM MODEL AND DESCRIPTION

In this section, the mathematical model of PMSM, Inverter, sensors, and controller are described

Model of the PMSM

A PMSM with multiple pole pairs has a stator winding composed of an equitable number of sets of coils. It is convenient to simply take into account one pole pair for the purposes of analysis because the criteria for PMSM with only one pole pair are the same as those with multiple pole pairs. A cross-section of a three-phase PMSM is schematically represented in Fig. 3.1 below, along with an α-β reference frame [2].

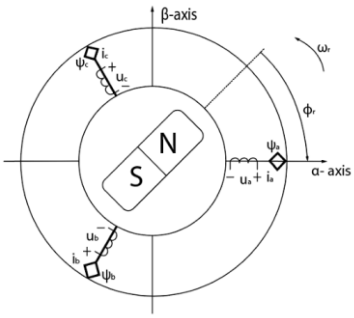

Fig. 3.1 View of a three-phase PMSM [2].

The PMSM mathematical model in the rotor rotating d-q reference frame could be expressed as:

$$\frac{di_d}{dt} = \frac{1}{L_s}(V_d - Ri_d + \omega L_s i_q) \quad (1)$$

$$\frac{di_q}{dt} = \frac{1}{L_s}(V_d - Ri_q - \omega L_s i_d - \omega\psi) \quad (2)$$

Where Vd and Vq, are the d and q axis stator voltages, i_d and i_q are the d and q axis stator currents, R is the stator resistance, Ls is the stator inductance, ω is the rotor angular velocity, and ψ is the permanent magnet flux linkage.

When it comes to angular position and velocity, the PMSM rotor's dynamics are determined by:

$$\frac{d\theta}{dt} = \omega \quad (3)$$

$$T_e = 1.5P[\psi i_q + (L_d - L_q) i_d i_q] \quad (4)$$

$$\frac{d\omega}{dt} = \frac{1}{J} T_e \quad (5)$$

Where J is the moment of inertia of the rotor [3].

A. Clark-park Transformation

Two key tools are necessary to create an effective controller for controlling three-phase PMSM: Clark Transformation and Park Transformation.

Clark Transformation (αβ transformation) represents a feasible analysis of three-phase electrical systems. Three-phase a, b, and c components that are evenly shifted by 120° into a two-phase system are mapped using the Clark transform. Two orthogonal components α and β serve as the representative for the new rotating vector. The space vector consists of a real (α) and imaginary (β) part, which represents two sinusoids shifted by 90° in time [4] as shown in Fig. 3.2.

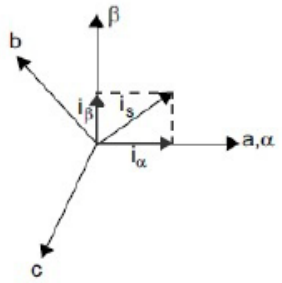

Fig. 3.2 Clark Transform for current [4].

As illustrated in figure 3.2 the Clark transformation can be defined as follows:

$$\begin{bmatrix} i_\alpha \\ i_\beta \end{bmatrix} = \sqrt{\frac{2}{3}} \begin{bmatrix} 1 & -1/2 & -1/2 \\ 0 & \sqrt{3}/2 & -\sqrt{3}/2 \end{bmatrix} \begin{bmatrix} i_a \\ i_b \\ i_c \end{bmatrix} \quad (6)$$

In the balanced three-phase system, the instantaneous sum of the three-phase current values will be zero. Utilizing Clark transform, we can measure only two components of the three-phase currents. Then the third component can be determined by calculation. In this scenario, the hardware cost is reduced as only two current sensors are needed.

The Park transformation transforms a stationary system into a rotating system known as synchronous coordinates or d-q coordinates. The space vector's instantaneous angle will be referenced to the θ angle. Analysis and control are made simpler by this transform, which makes the rotating vectors resemble DC quantities [4]. Fig. 3.3 Illustrates Park transform.

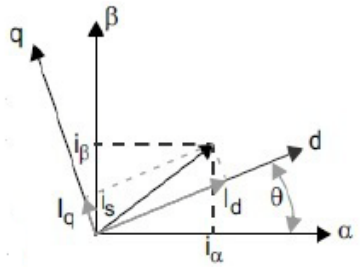

Fig. 3.3 Park Transform for current [4].

A new set of reference axes known as d and q is defined by the Park transformation. They rotate around the stationary αβ reference frame with a constant angular frequency ω. The transition from the stationary system to the synchronous rotating system is defined as:

$$\begin{bmatrix} i_d \\ q \end{bmatrix} = \begin{bmatrix} cos\theta & sin\theta \\ -sin\theta & cos\theta \end{bmatrix} \begin{bmatrix} i_\alpha \\ i_\beta \end{bmatrix} \quad (7)$$

In case of direct conversion from the three-phase system (abc) to the synchronous system (dq) -Which we will employ in our control system, the equation is given by:

$$\begin{bmatrix} i_d \\ q \end{bmatrix} = \begin{bmatrix} cos\theta & \cos(\theta + \frac{2\pi}{3}) & \cos(\theta - \frac{2\pi}{3}) \\ -sin\theta & -\sin(\theta + \frac{2\pi}{3}) & -\sin(\theta - \frac{2\pi}{3}) \end{bmatrix} \begin{bmatrix} i_a \\ i_b \\ i_c \end{bmatrix} \quad (8)$$

Three-Phase Inverter

The VSI (voltage source inverter) has a DC input voltage V_{dc}. Typically, the magnitude of this DC input voltage is constant. The inverter will use this DC input voltage to provide AC output voltage, where the magnitude and frequency can be varied. The Schematic is shown in fig. 3.4.

DOI: 10.17667/riim.2023.02

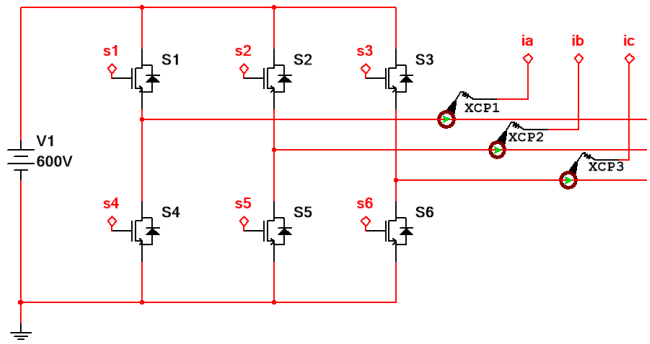

Fig. 3.4 inverter schematic.

The inverter is represented by ideal switches. The outputs of the SPWM component inside the controller drive the switches' gates. The inverter comprises three legs and six switches, as shown in figure 3.4. There are upper and lower switches on each leg. It is not possible to turn both the top and lower switches on or off simultaneously. As a consequence, each leg can be in either the top switch on lower switch off, or the top switch off lower switch on condition. Thus, There are eight different operating modes for three legs.

Gain	***Rise time***	***Overshoot***	***Settling time***	***Steady-state error***
K_p	Decrease	Increase	Small change	Decrease
K_I	Decrease	Increase	Increase	Decrease significantly

SPWM

One of the most widely used PWM techniques is SPWM (sinusoidal pulse width modulation), which has the advantage of lowering inverter harmonics. The concept is that three sinusoidal waves are employed as reference signals for a three-phase inverter with a phase shift of 120°. In SPWM modulation, the carrier wave is a triangle wave, and the modulation signal is a sinusoidal wave. The theory states that in order to obtain logical signals S_{1-6}, three-phase sinusoidal reference voltages (V_{aref}, V_{bref}, and V_{cref}) created by a current controller are compared with carrier waves. figure 3.5 below illustrates the principle.

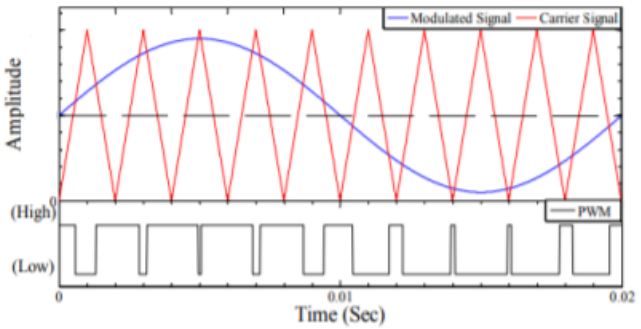

Fig3.4 Illustration of the PWM generation by comparison of modulation signal with carrier signal [5].

PI Controller

Feedback control is a control approach that utilizes information from measurements. There are two types of feedback, positive and negative. To control the system based on the incoming feedback, a PID controller is implemented. In our scope, we will only deal with the PI part. The PI controller can be described as a controller that considers both present and past errors.

The role of the proportional controller (PC) depends on the present error, the steady state error tends to depend inversely on the proportional gain. The proportional response can be tuned by multiplying the error by a constant K_p, called the proportional gain. The proportional term is given by:

$$P = K_p.error(t) \tag{9}$$

The proportional gain shortens the rise time, however, a very high proportional gain will make the system unstable. So, proportional gain can't solely eliminate the steady-state error.

The Integral controller (IC) is proportional to both the magnitude of the error and its duration. Therefore, the accumulated offset that needs to be corrected is calculated by adding up the instantaneous errors over time. Consequently, the steady-state error is eliminated by the integral controller K_I, but the transient response could get worse[6]. The integral term is given by:

$$I = K_I.\int_0^t error(t)dt \tag{10}$$

Table II below summarize the effect of both proportional and integral controller on the system.

TABLE II. PI CONTROLLER IN A CLOSED LOOP SYSTEM

Performance Metrics

Performance metrics enable system performance to be evaluated. Performance metrics are described as quantifiable measure that shows how effectively the PI controller is performing in the system. Through the use of this technique, it is possible to create an "optimum system" and tune the system's PI parameters to satisfy the needed specifications. For a PID- controlled system, there are often four metrics to depict the system performance ISE, IAE, IATE, and MSE [7]. In our scope, we will deal with the first two metrics, ISE, and IAE.

ISE means the integration of the square of the error over time. Larger errors will have a greater impact on ISE than smaller ones (since the square of a large error is much bigger). Control systems that aim to reduce ISE tend to quickly eliminate large errors, but they can tolerate persistent small errors for an extended period. Frequently, this leads to fast responses but with oscillation and low amplitude. ISE can be described as the following:

$$ISE = \int_0^\infty (error(t))^2 dt \tag{11}$$

IAE stands for the integration of the absolute error over time; it does not give any of the errors in the system's response any weight. Though typically with less sustained oscillations, it tends to produce a slower response than ISE optimum systems. IAE can be described as the following:

$$IAE = \int_0^\infty |error(t)|dt \quad (11)$$

IV. THE EXPERIMENT AND TESTS PERFORMED

On our PMSM in this experiment, we will apply a vector control approach known as decoupling or field-oriented control (FOC). This technique decouples the three-phase stator current into a two-phase d-q axis current, with one phase providing flux and the other producing torque [8]. The commutator maintains the field flux of a DC motor, which in this case is the stator flux, and the armature flux (rotor) mechanically orthogonal. When the fields are orthogonal, armature flux does not affect field flux, and the motor torque responds instantly to a change in armature flux or, more equivalently, armature current. The field flux (which is now in the rotor) rotates in an AC motor, but the FOC controller rotates the armature (stator) flux so that the armature and field flux remain orthogonal; hence, the AC motor acts like a DC motor [9]. Consequently, this leads to if we make the (*d*) component equal to zero then the electrical torque equation (4) becomes:

$$T_e = 1.5P(\psi i_q) \quad (12)$$

Hence, the electrical torque now is directly proportional to i_q, and a constant torque is obtained by ensuring that i_q is constant. Thus, the torque control becomes faster and simpler. The constant air gap flux required up to rated speed. Vector control is thus only conceivable when the instantaneous rotor flux is precisely known. In the PMSM, the rotor flux is determined solely by the rotor position.

Multisim Model and Simulation

For our experiment, we first modeled our power circuit via Multisim software by National Instruments. figure. 4.1 below shows the main component of the power circuit.

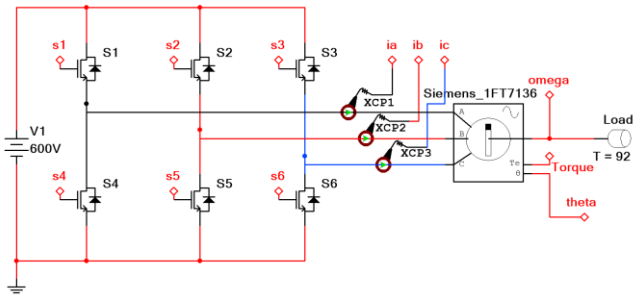

Fig. 4.1 Power circuit model.

The inverter is modeled using ideal switches operating at a gating signal of 5V, the gates of the switches are driven by the output of the SPWM component inside the controller. The current clamps are used to convert the phase currents to voltage signals which are processed by the controller. The three-phase currents generated from the inverted are then fed to the PMSM. We get the speed and the position of the rotor as feedback for the controller. The torque is also measured to evaluate the performance of the system. Figure. 4.2 below shows the main components of the control circuit.

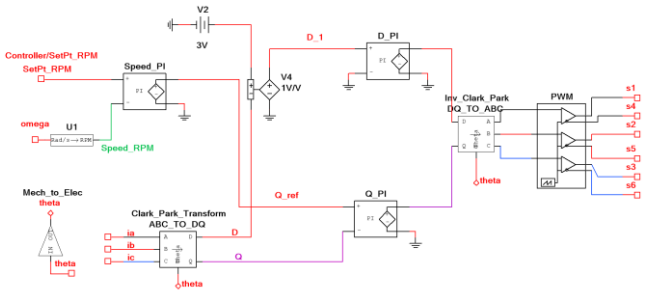

Fig. 4.2 Control circuit model.

In the control model, all voltages are treated as abstract signals, the three voltages measured from i_a, i_b, i_c are fed into the Clark-Park transform, along with the instantaneous position of the rotor (theta), it's important to note that the output of the position sensor gives the mechanical angle, hence, the angle must be converted from mechanical to electrical before it's fed into Clark-Park as following:

$$\theta_e = \frac{P}{2}\theta_m \quad (13)$$

As *P* is the number of poles, the output of the Clark-Park block is the d and q components, the q components are then fed to the Q PI controller which has a reference fed from the speed PI controller which controls the error between the reference speed and the actual speed. The d component is fed to the D PI controller which eliminates the direct component to be near zero, the outputs from D and Q PI controllers are then fed into the inverse Clark-Park transform block to return to their original a, b, and c components which goes to the SPWM to generate the switching signals that operate the switches on the inverter. Hence, the output voltage amplitude of the SPWM is set to 5V with a reference signal amplitude of 40 and. Our test is performed in a time range from zero to 0.3 seconds with an initial time step of 1ms and a maximum time step of 10ms. Figure. 4.3 shows the speed performance before tuning the controllers and SPWM.

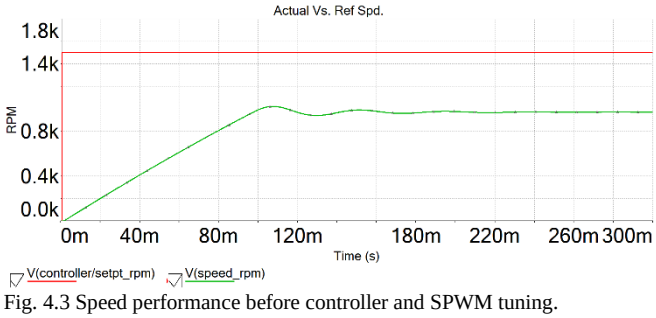

Fig. 4.3 Speed performance before controller and SPWM tuning.

As shown in Figure 4.3 above, the actual speed is way far from the desired speed as it reached 1000rpm with a lot of ripples before reaching the steady state. Figure. 4.4 shows the speed performance after tuning the SPWM.

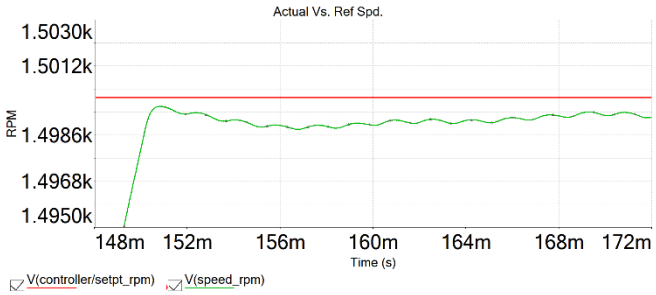

Fig. 4.4 Speed performance after SPWM tuning.

The motor speed nearly reached the desired speed after 150.5ms but with significant error and ripples before reaching the steady state. The next step is to tune the PI controllers. To evaluate the effect of the tuning we calculated the ISE and IAE for each iteration to perceive the enhancement in the performance and notice the effect caused by tuning each gain as shown in table III.

TABLE III. PI TUNING ITERATIONS FOR MULTISIM

I	Gain Value						Perf. Metrics	
	Speed Controller		*I_d Controller*		*I_q Controller*		*ISE*	*IAE*
	Kp	*Ki*	*Kp*	*Ki*	*Kp*	*Ki*		
0	10	0.30	8	0.2	10	0.30	104863.56	105.84
1	15	0.30	8	0.2	10	0.30	104863.55	105.83
2	20	0.30	8	0.2	10	0.30	104863.55	105.82
3	30	0.30	8	0.2	10	0.30	104863.55	105.81
4	45	0.30	8	0.2	10	0.30	104863.55	105.81
5	45	0.30	8	0.2	15	0.30	104490.16	105.48
6	45	0.30	8	0.2	20	0.30	103855.42	104.45
7	45	0.30	8	0.2	30	0.30	103130.00	103.49
8	45	0.30	8	0.2	45	0.30	102687.36	102.88
9	45	0.30	8	0.2	60	0.30	102486.77	102.60
10	45	0.30	8	0.2	75	0.30	102364.73	102.42

The performance metrics have decreased which indicates higher performance mainly by increasing the proportional gain of both the speed controller and the I_q controller. We noticed that the proportional gain of the Speed controller has a higher effect in IAE where there is an imperceptible effect on ISE, and vice versa for the proportional gain of the I_q controller. Figure 4.5 shows the tuning effect on performance.

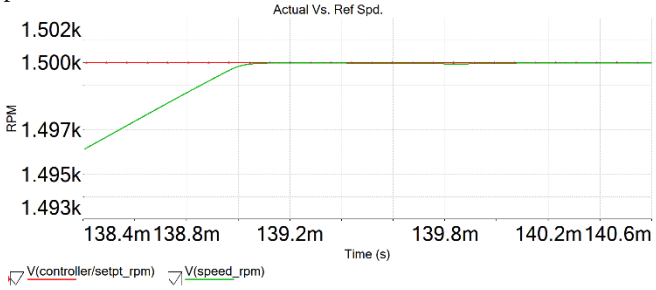

Fig. 4.5 Speed performance after PI controllers tuning.

After tuning the PI controllers, it's shown that the motor has reached the desired speed within 139.1ms which is faster than the response before tuning which was at 150.5ms, this rise time improvement is mainly due to tuning of the proportional gain, it's also noticed that the ripples have been significantly eliminated due to tuning of the integral gain.

LabVIEW Model and Simulation

After testing our model on Multisim, we have implemented it into the LabVIEW software by National Instruments, for more accurate results, as LabVIEW allows us to perform simulations in much smaller step-time in a significantly shorter time in comparison with Multisim, as the step-time decreases, the results become more accurate. Figure 4.6 below shows the block diagram of our model.

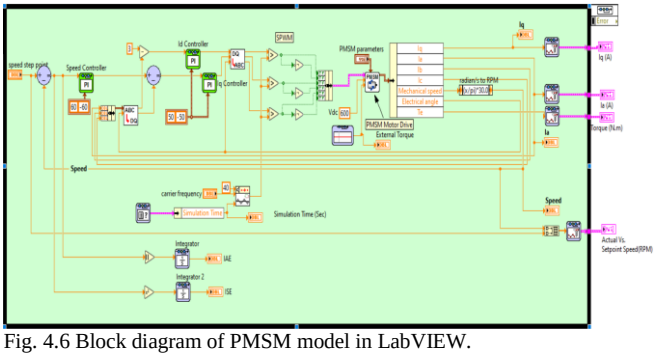

Fig. 4.6 Block diagram of PMSM model in LabVIEW.

Another feature of LabVIEW is that it has a front control panel beside the block diagram, with a user-friendly GUI that enables simpler control and observation, as illustrated in figure 4.7 below.

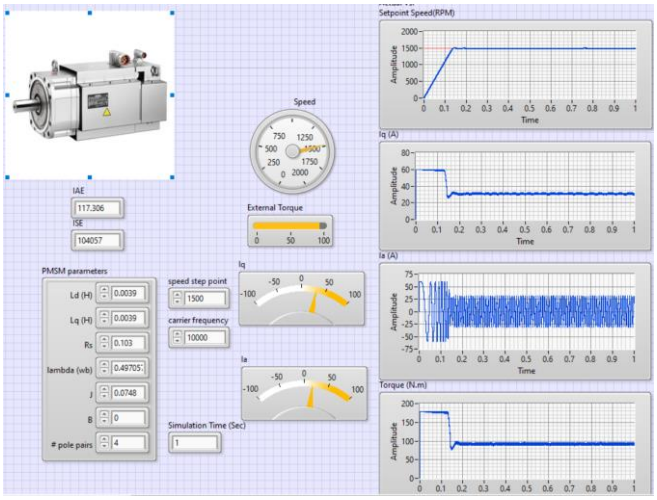

Fig. 4.7. Front panel of PMSM model in LabVIEW.

Our test is performed on a time range from zero to 1 second with a step time of 0.5 microseconds under the same conditions applied on Multisim, Fig. 4.8 shows the speed performance before tuning SPWM and the PI Controllers.

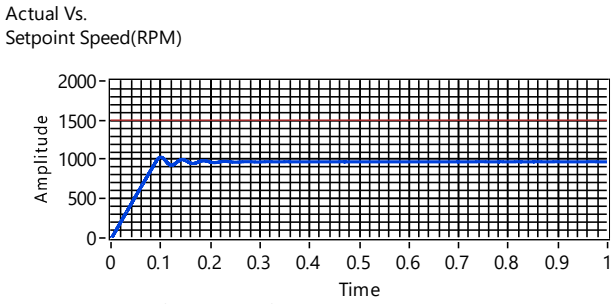

Fig 4.8. Speed performance before controller and SPWM tuning.

As shown in Fig. 4.8, the speed barely reached 1000 rpm with a lot of ripples before reaching the steady state value. In the next step, we've tuned the PWM and PI controllers, to observe the effect of PI controllers tuning, we applied iterations and measured the ISE and IAE for each iteration, the same as we did for Multisim Model. Iterations are shown in table IV.

TABLE IV. PI TUNING ITERATIONS

I	Gain Value						Perf. Metrics	
	Speed Controller		*Id Controller*		*Iq Controller*		*ISE*	*IAE*
	Kp	*Ki*	*Kp*	*Ki*	*Kp*	*Ki*		
0	10	0.30	8	0.2	10	0.30	107160.00	108.49
1	15	0.30	8	0.2	10	0.30	107160.00	108.40
3	20	0.30	8	0.2	10	0.30	107160.00	108.31
5	45	0.30	8	0.2	15	0.30	105704.00	106.26
7	45	0.30	8	0.2	30	0.30	104319.00	104.36
9	45	0.30	8	0.2	60	0.30	103650.00	103.44
11	45	0.30	8	0.2	95	0.80	103406.00	103.12
13	45	0.30	8	0.6	95	0.80	103405.00	103.12
15	45	0.30	13	1.0	95	0.80	103404.00	103.08
16	60	0.30	13	1.0	95	0.80	103404.00	103.08

According to the table above, the ISE and IAE have decreased during the iterations which indicates a high-performance profile, the proportional gains of the speed controller and Iq controller contributed to decreasing the ISE while the main effect of Integral gain is decreasing the IAE. Figure 4.9 below shows the performance after tuning the SPWM and PI controllers.

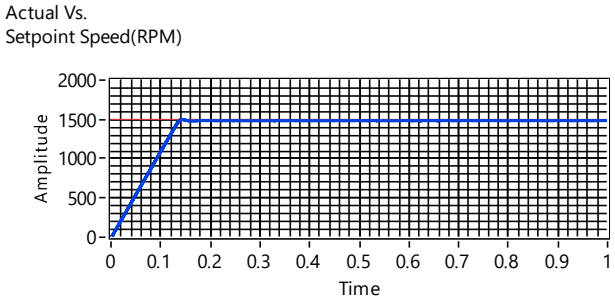

Fig. 4.9 Speed performance after controller and SPWM tuning.

After tuning, it's shown that the motor has reached the desired speed within 130ms and the ripples are significantly eliminated. Figures 4.10, 4.11, and 4.12 show the profile of the phase current, Iq, and torque respectively.

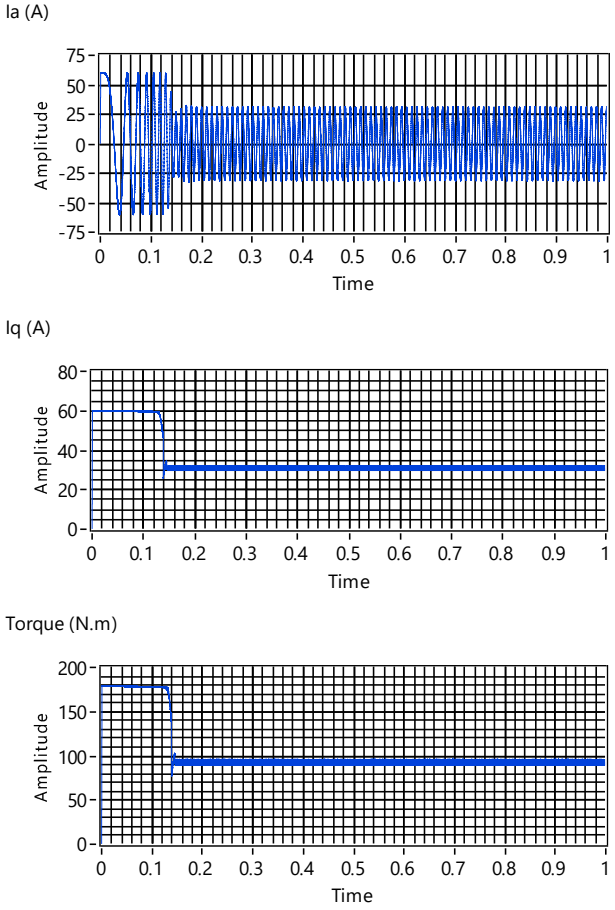

Fig 4.10, 4.11, 4.12 Phase current, Iq, and Torque profiles.

Figure 4.10 demonstrates that when a motor is starting, the current is higher than the rated current; yet, as the motor reaches the desired speed, the current drops to match the motor's rated current of 25A. Figures 4.11 and 4.12 show how the torque profile is directly connected to the I_q profile which confirms the equation (12) discussed earlier.

V. EVALUATION OF CONTROLLER TUNING AND TEST CONDITIONS

In our experiment, we can notice that the proportional gains of the speed controllers and I_q controllers have a higher effect on improving the system performance along with the integral gains of the I_d controller and I_q controller. This combination of proportional gains and integral gains tuning allows the balance between having a shorter rise time and not having an overshoot and ripples during the steady state. It's also noticed that there is a limit to increasing the proportional gain as it may lead to overshoot as a consequence of the shorter rising time. Figure 5.1 illustrates ISE and IAE changes over the iterations.

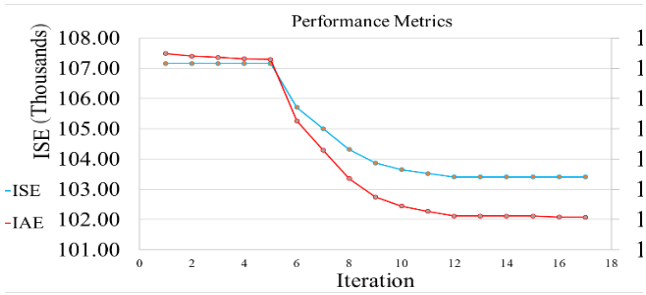

Fig. 5.1 Performance metrics over tuning iterations.

VI. Conclusion

In this paper, vector control has been described in adequate detail and implemented on our PMSM model. It allowed us to transform a complex and coupled AC model into a simple linear system. The time-varying abc currents are decoupled into two rotating vectors d-q using Clark-Park transformation to simplify the calculations and control. So, we had independent control of torque and flux, similar to a DC motor. Vector control results in a fast dynamic response, good transient, and steady-state performance, with high torque and relatively low current at startup along with high efficiency. The experiment met our expectations as the performance matched the rated values and the torque profile confirmed equation (12). It was noticed that changing integral gains of I_d and I_q controllers reduced the performance quality whereas the proportional gains of speed and I_q controllers have noticeably improved it. The best performance was achieved in the 10^{th} iteration of the Multisim simulation and the 16^{th} iteration of the LabVIEW simulation.

References

[1] SIEMENS, "SIMOTICS S-1FT7 Synchronous motors configuration Manual," Siemens AG, Nurnberg, 2018.

[2] W. Han, Simulation model development of electric motor and controller, Gothenburg: Chalmers University of Technology, 2017.

[3] S. H. Hosseini and M. Tabatabaei, "IPMSM velocity and current control using MTPA based adaptive fractional order sliding mode controller," *Engineering Science and Technology, an International Journal*, vol. 20, no. 3, pp. 896-908, 29 April 2017.

[4] A. A. A.-R. Ahmed, Digital Control Techniques for Grid-Connected Inverters, Cairo: Ain Shams University, 2013.

[5] M. Issa, K. Ait-Yahia, R. Lepage, H. Ibrahim, A. Ilinca and M. Ghandour, "Integrated A Variable Frequency Drive for a Diesel-Generating Set using the Genset-Synchro Concept," *International Journal of Engineering Research & Technology*, vol. 8, no. 8, pp. 232-239, 2019.

[6] K. A. Tehrani and A. Mpanda, "PID Control Theory," in *Introduction to PID Controllers - Theory, Tuning and Application to Frontier Areas*, R. C. Panda, Ed., Rijeka, InTech, 2012, pp. 213-228.

[7] Y. K. Soni and R. Bhatt, "BF-PSO optimized PID Controller design using ISE, IAE, IATE and MSE error criteria," *International Journal of Advanced Research in Computer Engineering & Technology*, vol. 2, no. 7, pp. 2333-2336, 2013.

[8] K. Jash, P. K. Saha and G. K. Panda, "Vector Control of Permanent Magnet Synchronous Motor Based On Sinusoidal Pulse Width Modulated Inverter with Proportional Integral Controller," *Int. Journal of Engineering Research and Applications*, vol. 3, no. 5, pp. 913-917, 2013.

[9] D. Ocen, Direct Torque Control of a Permanent Magnet Synchronous Motor, Stockholm: KHT Signals, Sensors and Systems, 2005.